May 18, 2019

Dear Dr. Chambon,

We are grateful that the referees agreed to review our revised manuscript (tc-2018-198), titled *Monitoring of Snow Surface Near-Infrared Bidirectional Reflectance Factors with Added Light Absorbing [Particles]*, once again. We appreciate their new comments and revised the manuscript accordingly. We believe that their suggestions continue to improve the structure and readability of the paper.

In the following attachment, we respond to the referees' comments, as before. We begin with our response to Dr. Dumont and then address Anonymous Referee #3's comments. Following our point-by-point response is the marked-up manuscript showing our changes, which appear extensive due in large part to the rearranging of paragraphs in the introduction and in section two. This rearrangement is necessary to fully address Dr. Dumont's remarks regarding the unclear motivation for the study as well as their suggestions for improving the consistency within sections. Finally, we carefully checked the manuscript for typos and misnomers, which led to a few changes including added references, updated terminology, and refined equations.

We appreciate your complimentary report and hope that you find our latest revision more polished and ready for publication in *The Cryosphere*.

Sincerely,

Adam Schneider
amschne@umich.edu

We appreciate Dr. Dumont's second review. In addressing their comments, revising continues to improve the overall structure of the paper. Here, Dr. Dumont points out some remaining concerns, the most critical of which addresses the unclear motivation for the objectives stated in the introduction. In the revised manuscript, we rearranged parts of the introduction to narrow in on the foci of the study. This includes a revised paragraph that better presents our motivation, as further described below (see comment 7).

1. *Title, abstract and everywhere in the text : LAI can be a misleading acronym, the use of LAP (light absorbing particle) is maybe to be preferred*
   We changed all instances of light absorbing impurities (LAIs) to light absorbing particles (LAPs), including in the title.

2. *P1, Line 20 – Picard et al., 2009 did not use only spherical ice particles*
   We removed the reference to Picard et al., 2009 from this part of the Introduction, but still cite their similar results in the Results and Discussion.

3. *P1, Lines 14-15 – LAP can also be living particles, maybe the recent review from Skiles et al., NCC on LAP in snow can be added as reference in the introduction*
   Skiles, S. M., Flanner, M., Cook, J. M., Dumont, M., & Painter, T. H. (2018). Radiative forcing by light-absorbing particles in snow. Nature Climate Change
   In reference to biological LAPs, we added "microbes" to the list of LAPs in the introduction and also included a reference to Skiles et al., 2018.

4. *P2, Line 15 – References to SSA profilers such as ASSSAP, POSSUM or SMP are missing*
   Arnaud, L., Picard, G., Champollion, N., Domine, F., Gallet, J.C., Lefebvre, E., Fily, M. and Barnola, J.M., 2011. Measurement of vertical profiles of snow specific surface area with a 1cm resolution using infrared reflectance: instrument description and validation. Journal of Glaciology, 57(201), pp.17-29.
   Proksch, M., Löwe, H. and Schneebeli, M., 2015. Density, specific surface area, and correlation length of snow measured by high-resolution penetrometry. Journal of Geophysical Research: Earth Surface, 120(2), pp.346-362.
   Because the POSSUM is very similar to the NERD, we added a sentence that briefly describes its SSA retrieval method and also cites Arnaud et al., 2011. We also included the POSSUM in the context of our motivation and now reference the authors in the description of the NERD in section 2.2. We are unsure, however, where to include Proksch et al., 2015.

5. *P2, lines 16-18 – "in isothermal snow, highly faceted snow grains" this sentence seems a bit weird to me. Isothermal metamorphism and coarsening also happens for non faceted crystals.*
   We rephrased this sentence, removing the "...faceted snow..." descriptor. We also moved this revised paragraph before the introduction of SSA measurement methods to provide readers context for how snow SSA is used to evaluate snow metamorphism.

6. *P2, lines 25 and below – The beginning of the paragraph is a bit difficult to follow. I agree with the general idea I don't see any clear link with the objective of the paper and I would*

remove it. I would also reverse the order of the two objectives in accordance with the paper structure.
We rewrote the beginning of the paragraph to clarify the motivation for our study. As suggested, we also reversed the order of the objectives to align with the rest of the paper.

7. *General remarks on the introduction: I am not all questioning the utility of the instrument and measurements but from the sole information provided by the authors, it is a bit difficult to understand why a new instrument is needed and what are the specifications. Regarding the objective one, I would also recommend that this quantification of snow albedo feedback impact on metamorphism be justified in light of previous studies and measurements.*
To clarify the purpose of the study, we added a couple sentences regarding the limited access to appropriate snow SSA instruments. In doing so, we attempt to find the optimal balance of motivating the need for the new instrument without implying that snow SSA instruments do not exist. We hope that the revised manuscript sufficiently motivates the desire for an inexpensive instrument that can be used to monitor snow surface SSA with added LAPs, but does not suggest that established snow SSA measurement methods are inadequate.

8. *Maybe start by section 2.3 (modeling) and then 2.2 and 2.4 (two "measurements" sections)*
This is a good suggestion that improves the consistency of the overall structure of the paper. We are particularly thankful for this suggestion. We rearranged section two to begin with the numerical simulation methodology.

9. *Section 2.2.2 lines 24-26 – Is it possible to provide the absolute changes calculated in SSA, also maybe give explicitly value of tau and n.*
Yes. This information is now included in the text at the end of section 2.3.1.

10. *Section 2.4.2 what is the approximated mass of dust that was spread on the snow surface? 30g m-2 ? How does it compare to values from Skiles and Painter, 2017?*
Yes. We deposited 30 grams of filtered sand over 1 square meter of snow. This dust flux was the largest dust deposition event observed by Skiles and Painter, 2017. We clarified this a bit in the text.

11. *P7, lines 6-9 – What's the point of the last sentence? It needs to be removed or detailed a bit more.*
For a fixed particle size, differences in Monte Carlo simulated reflectances across particle shape seem to vary with the particle's asymmetry parameter. This intuitive hypothesis is mostly speculative from Monte Carlo results beyond those presented in the manuscript. As such, we removed the sentence in question.

12. *P7 lines 10-15 – The information discussed here seems quite redundant with section 3.2, is it possible in sake of clarity to remove redundancies?*
This is a helpful comment that motivated us to rearrange parts of sections 3.1 and 3.2. In the revised manuscript, section 3.1 presents results strictly from Monte Carlo simulations. In section 3.2, we present snow BRF and SSA measurements and then compare modeling results with measurements. In revising these subsections, we removed redundancies and

improved the continuity of the presentation of results and discussion.

13. *P7 lines 31 – This is also in line with more theoretical studies such as Kokhanovsky and Zege, 2004 and Malinka, 2014.*
Kokhanovsky, A.A. and Zege, E.P., 2004. Scattering optics of snow. Applied Optics, 43(7), pp.1589-1602.
Malinka, A.V., 2014. Light scattering in porous materials: Geometrical optics and stereological approach. Journal of Quantitative Spectroscopy and Radiative Transfer, 141, pp.14-23.
We added a reference to Malinka, 2014 in the description of the Monte Carlo model with added details to better present our model in the context of similar studies. We also added a reference to Kokhanovsky and Zege, 2004, making note of the agreement between their theoretical framework and our modeling results.

14. *P9, line 16 "realistic", maybe a bit more details/references is required.*
We changed "realistic" to "extreme" to better summarize our findings.

15. *P9, lines 18-19 – "initiated melting" depends on the weather conditions (not only clear/cloudy), and the snow albedo feedbacks is also present before melting.*
We removed this speculative sentence.

16. *P3 line 13-14, the authors stated that the measurement is not sensitive to small BC concentrations, but is it sensitive to the large amount of BC or dust used in the experiments ?*
Large amounts of added BC and dust did have a (small) direct effect on measured BRFs. We added details regarding measurements conducted soon after the initial application of the LAPs to the text, including how much large LAP applications affected BRF measurements.

17. *P1, Line 1 – snow albedo -> broadband snow albedo*
We added the word "broadband."

18. *P1, Lines 11-12 – the last sentence should maybe be move after measurements (line 8)*
We moved the last sentence to after the measurement summary.

19. *P1, Line 9 -10 – "These findings ..." as stated in the main text, the results here is not a new finding so maybe rephrase*
As such, we changed "These findings..." to "These results..."

20. *P1, Line 22 – "its effective radius" -> "its effective radius, Re"*
We now define "sphere effective radius, r_e," verbatim at the beginning of the second paragraph in the introduction.

21. *P2, lines 23-24 – I would remove this last sentence,*
We removed this sentence.

22. *P3, line 20 – "Flat paint" the details provided in the response to reviewer are maybe useful in the text of the paper too.*

We added a few details regarding how we tested the black paint at the end of the second paragraph in section 2.2.

23. *P4, line 3 – "at most a couple of centimeters" a few references would be useful for the reader here.*
    We added references to Smith et al., 2018, Kaempfer et al., 2007, Grenfell et al., 1994, and Brandt and Warren, 1993. They provide further information regarding volume scattering in snowpack.
24. *P5, line 1 - "were conducted" -> "were conducted only" ??*
    We conducted contact spectroscopy measurements only for two snow samples (DH_2016 and RG_2015). We rephrased this sentence to clarify this point.

25. *P5, line 5 - "at random" -> maybe one word is missing*
    We revised the section (2.1) relevant to this comment and removed the poor phrasing.

26. *P5, line 13 - typo for snowpacks*
    We changed all instances of the typo "snow pack" to "snowpack."

27. *P5, lines 15 -20 – maybe explain why a different choice is conducted for spheres and for the other shapes.*
    We added the detail that we use the HG phase function for spheres to improve computational efficiency.

28. *P6 – first paragraph. I am a bit confused by all the different numbers of photons. In the end, 1,000,000 photons was chosen for the simulations ? maybe just rephrase this section.*
    There are indeed a lot of photons. We revised this paragraph, now at the end of section 2.1, to hopefully mitigate any lingering confusion.

29. *P6, line 12 – "were sifted" -> which diameter ?*
    We added details regarding how particles were filtered (roughly 1 mm diameter).

30. *P6, line 22 – I don't think that diffuse radiation is isotropic for cloudy conditions. Maybe rephrase "nearly isotropic".*
    We removed the term "isotropic," instead using only "diffuse."

31. *Figure 5* [4?] *is quite difficult to read, maybe the model results can be shown in black without markers to ease the comparison with the NERD measurements?*
    We changed the colors of the modeling results in figures 3 and 4 to black, for Monte Carlo results, and gray, for SNICAR results. We kept the markers, however, to more easily distinguish between shape habits.

32. *P8, lines 19-22 , "As expected", "typically" : can you provide any reference for that ?*
    We cannot provide any references. As such, we removed language suggesting that higher snow SSA derived from contact spectroscopy than from X-CT is an expected result.

33. *P8, line 33 – "little to no effect" -> during the time of the experiment? "only" 16 hours*
    We clarified that the results from this experiment pertain only to the 16 hours during which it lasted.

34. *Figure 6 and Figure 7 : it is quite difficult to guess what are the limits of the errors bar, can it be modified ?*
    We shifted data in figures 6 and 7 by 15 minutes, for added BC experiments, and by 30 minutes, for added dust experiments. This actually better represents measurement data, as roughly 15 minutes elapsed between data collection between these snow plots.

35. *Legend of figure 7, the labelling is different for the upper and lower panels, maybe homogenize.*
    We homogenized the labeling, as suggested.

We are grateful that Anonymous Referee #3 decided to review our revised manuscript, as their first review motivated us to change the main foci of the paper. Without their thoughtful suggestions, the presentation of our key results would have been obscured by an ineffective writing style. We are glad that they believe the revised manuscript is improved and wish to give credit to them for helping us better communicate our results. Below, we respond to their enumerated comments.

1. *I think the authors present a streamlined and much-improved revised version of their manuscript. They also addressed in great detail the comments I had about the initial manuscript, which I appreciate. I only have a few minor comments regarding the revised manuscript (see specific comments below).*
   Thank you for reviewing our manuscript(s)! We addressed the below specific comments in a second revision.

2. *While the main focus of the manuscript has shifted (and the manuscript benefits from this), I would still encourage the authors to tackle a more detailed assessment of the snow SSA measurement uncertainties for their NERD in the future (as they seem to allude to in the final sentence of their conclusions). Unfortunately, such uncertainty analyses are still not always provided when a(ny) novel measurement technique is introduced, yet they can be highly valuable for the application of a(ny) novel measurement technique, especially when trying to interpret initially puzzling measurement results from both a qualitative and a quantitative perspective or for an inter- comparison of different measurement techniques or when comparing in situ measurements and remote sensing retrievals. For snow SSA measurements with the NERD, one crucial component that should be included in more detail in a possible future study is how the natural variability of snow at and near the surface and especially within the NERD measurement volume may affect derived snow SSA values.*
   While this comment mainly concerns future work, in the conclusions, we added "...investigation of the natural variability of snow near the surface" to the list of topics to include in a follow on study.

3. *page 1 line 23: I do not fully understand the different expressions for sphere effective radius r_eff and Re; is one definition based on the ice surface area and the other one on the projected area? Maybe the authors could either briefly clarify the difference or only introduce one of the two effective radii here.*

Yes. The definitions differ based on the surface area versus projected area. To eliminate potential confusion, as suggested, we now only introduce one effective radius (r_e) defined by the surface area.

4. *p.2 l.7, 9 and 12: I would suggest to remove the word 'accurate', because the usage of the qualifier 'accurate' should also include information on how accurate the measurement method is (i.e., accurate ... with an uncertainty of XYZ % or with an accuracy of better than xyz m2/kg, for example). If such information about the measurement uncertainty cannot be obtained or summarized easily, I would just leave out this qualifier.*
   Throughout the manuscript, we removed all instances of the qualifier "accurate" when used without corresponding uncertainty quantification.

5. *p.4 l.2ff: To illustrate this point, the authors could provide the first figure that they included in their author response in a Supplement to the article or in a second Appendix section, or they could possibly cite a previous study that shows this shallow penetration depth of long-NIR-wavelength radiation in snow.*
   We cited previous studies by Kaempfer et al., 2007, Smith et al., 2018, Grenfell et al., 1993, and Brandt and Warren, 1993, from which the shallow penetration depth at longer NIR wavelengths can be inferred. If the editor considers it necessary, we will include a supplement that further illustrates this point, as suggested.

6. *p.5 l.1: Is '1 nm' correct? This should probably be 1 μm (or 1000 nm).*
   Thank you for brining this to our attention. Yes, it should indeed be 1 μm. We corrected this mistake.

7. *p.6 l.24: What is 'just a pinch' of BC? According to the caption of Figure 7, this seems to be < 1 g. I would suggest to add this value here as well: ..., just a pinch (< 1 g) of BC and 30 g of sand were deposited ...*
   As suggested, we inserted "(< 1 g)" as a rough quantification of the mass of BC used.

8. *p.10 l.8: Again, without further specifying 'accurate', e.g., a specific accuracy that the NERD aims to achieve, I would remove 'accurate' and rewrite the sentence, e.g.: ... are needed to fully characterize snow SSA measurements by the NERD (technique). Further investigation ...*
   Throughout the manuscript, we removed all instances of the qualifier "accurate" when used without corresponding uncertainty quantification (copied from response to comment 4, above).

9. *p.10 l.9: Similarly as above for 'accurate', I would suggest to remove the qualifier 'precise'. Alluding to 'quantitative uncertainties' already implies that the accuracy and precision of snow SSA retrievals will be the subject of the follow-on study.*
   By the way, I believe that such a study will be very valuable for the future application of the NERD and the interpretation of the measurement results.
   We removed this instance of "precise."
   Thank you! We are excited about the future development of the NERD and hope to continue with a refined quantitative uncertainty analysis, as suggested (and needed).

10. *Caption of Figure 3: Remove comma before droxtals.*
    Removed.

11. *Caption of Figure 6 + 7, and possibly in corresponding text of the article: I would suggest to replace 'standard errors' with 'standard deviations'.*
    Because each BRF measurement already averages 100 samples, we believe calculating standard deviations across the NERD BRF measurements are actually better described as "standard errors."

12. *Caption of Figure 7: Are the units of gm-1 correct, as in < 1 g m-1 and 30 g m-1? Maybe I do not fully understand, but units of g m-2 would make more sense to me.*
    Thank you for catching this. We corrected these units to gm^{-2}.

Monitoring of Snow Surface Near-Infrared Bidirectional Reflectance Factors with Added Light Absorbing ~~Impurities~~Particles

Adam Schneider[1], Mark Flanner[1], Roger De Roo[1], and Alden Adolph[2]

[1]Department of Climate and Space Sciences and Engineering, Climate & Space Research Building, University of Michigan, 2455 Hayward St., Ann Arbor, MI 48109-2143
[2]Physics Department, St. Olaf College, 1520 St. Olaf Ave., Northfield, MN 55057

Correspondence: Adam Schneider (amschne@umich.edu)

Abstract. ~~Snow~~ Broadband snow albedo can range from 0.3 to 0.9 depending on microphysical properties and light absorbing ~~impurity (LAI~~particle (LAP) concentrations. Beyond the widely observed direct and visibly apparent effect of darkening snow, it is still unclear how ~~LAI~~ LAPs influence snow albedo feedbacks. To investigate ~~the LAI~~ LAPs' indirect effect on snow albedo feedbacks, we developed and calibrated the Near-Infrared Emitting and Reflectance-Monitoring Dome (NERD) and monitored bidirectional reflectance factors (BRFs) hourly after depositing dust and black carbon (BC) particles onto experimental snow surfaces. After comparing snow infrared BRFs to snow SSA, we found that both measured and modeled snow infrared BRFs are correlated with snow SSA. These results, however, demonstrate a considerable uncertainty of $+/-$ 10 m^2kg^{-1} in the determination of snow SSA from our BRF measurements. The nondestructive technique for snow SSA retrieval presented here can be further developed for science applications that require rapid in situ snow SSA measurements. After adding large amounts of dust and BC to snow, we found more rapid decreasing of snow BRFs and SSA in snow with added ~~LAI~~ LAPs compared to natural (clean) snow, but only during clear sky conditions. These ~~findings suggest that the deposition of LAIs~~ results suggest that deposition of LAPs onto snow can ~~enhance snow metamorphism from direct solar irradiance via~~ accelerate snow metamorphism via a net positive snow ~~albedo feedback. The nondestructive technique for snow SSA retrieval presented here can be further developed for science applications that require rapid in situ snow SSA measurements.~~ grain-size feedback.

1 Introduction

~~Common light absorbing impurities (LAI) in snow include~~ Snow cover modulates Earth's surface energy budget by reflecting a large portion of the incident solar radiative energy flux. As snow melts, more absorptive surfaces are uncovered resulting in a positive feedback mechanism known as the snow albedo feedback (SAF) (Qu and Hall, 2007; Hall, 2004). Light absorbing particles (LAPs) within the snowpack, including elemental (black) carbon (BC), brown carbon, ~~and dustparticulate matter, all of which play an important role in the climate system (Bond et al., 2013; Qian et al., 2015). In particular, these LAI at the snow surface can reduce snow albedo and enhance snow melt via the snow~~ dust, and microbes, directly decrease snow albedo ~~feedback (Qu and Hall, 2007; Skiles and Painter, 2017). Hadley and Kirchstetter (2012) experimentally verify this effect and~~

~~confirm what Warren and Wiscombe (1980) and the widely used~~ which can initiate the SAF and accelerate snow melt (Bond et al., 2013; Qi . Hadley and Kirchstetter (2012) experimentally verified that the reduction of snow albedo due to BC is enhanced for larger snow grains, implying a possible positive "grain-size" feedback induced by impurities in the snow. This positive feedback can also be inferred from the spectral snow albedo models presented by Warren and Wiscombe (1980) and from the Snow, Ice, and Aerosol Radiation (SNICAR) model (Flanner et al., 2007, 2009)~~predict in that snow albedo reduction by BC is enhanced for larger snow effective radii. Numerical snow albedo studies, including those from Wiscombe and Warren (1980) , and Picard et al. (2009), typically model~~ . Generally, two-layer models that represent snowpack as a ~~semi-infinite medium of suspended spherical ice particles. These models are highly accurate for spectral snow albedo calculations when the snow effective radius is a tunable parameter. Spherical snow~~ collection of spheres can reproduce spectral hemispherical reflectances that compare well with observations (Grenfell et al., 1994).

Snow grain size is often quantified by its optically equivalent sphere effective radius, r_e, which is related to specific surface area~~(SSA) by its effective radius~~, SSA, such that SSA = 3/($\rho_{ice} r_e$), where ρ_{ice} ~~Re). Expressions of sphere effective radii, r_{eff} and Re, defined by ice particle surface area S versus ice particle projected area A, respectively, are equivalent for convex bodies (Vouk, 1948).~~

is the density of pure ice (917 kg/m^3 at 0° C). Snow SSA is defined as the total ice-air interfacial surface area S to ice mass m ratio, such that

$$\mathrm{SSA} = S/m = \frac{S}{\rho_{ice} V}, \tag{1}$$

expressed in terms of its total ice ~~volume~~ mass or volume, V ~~such that,~~

$$\mathrm{SSA} = S/m = \frac{S}{\rho_{ice} V},$$

~~where ρ_{ice} is the density of pure ice (917 kg/m^3 at 0° C) (Hagenmuller et al., 2016; Gallet et al., 2014).~~ (Hagenmuller et al., 2016; Gallet et . In snowpack with large temperature gradients, the diffusion of vapor causes snow SSA to decrease during the natural process of snow metamorphism (Flanner and Zender, 2006; Wang and Baker, 2014). In the absence of a temperature gradient, an isothermal snowpack with snow grains with low radii of curvature undergo coarsening in a process driven by the Kelvin effect. Ebner et al. (2015) show that measurements of snow SSA evolution in isothermal snow agree with the isothermal snow metamorphism modeling framework developed by Legagneux et al. (2004) and Legagneux and Domine (2005). These laboratory studies express snow SSA in isothermal metamorphism as a function of time t as follows,

$$\mathrm{SSA}(t) = \mathrm{SSA}_0 \left(\frac{\tau}{\tau + t} \right)^{1/n}, \tag{2}$$

for initial snow SSA_0 at $t = 0$ and adjustable parameters τ and n.

Snow SSA strongly affects absorption of infrared radiation. This relationship is evident from measurements of infrared reflectance that are highly correlated with snow SSA for various snow types (Domine et al., 2006). Among others, Gallet et al.

(2009) and Gallet et al. (2014) exploit this correlation in the ~~accurate~~ determination of dry snow SSA and wet snow SSA, respectively, using 1.31 µm directional hemispherical reflectance measurements (1.55 µm for measurements of snow SSA > 60 m^{2}kg^{-1}). Arnaud et al. (2011) present the Profiler Of snow SSA Using SWIR reflectance Measurement (POSSUM), which applies the theoretical formulations from Kokhanovsky and Zege (2004) and Picard et al. (2009) to derive snow SSA from hemispherically averaged bidirectional reflectance measurements. Other studies establish techniques to ~~accurately~~ obtain snow SSA using methane gas absorption (Legagneux et al., 2002) and X-ray micro-computed tomography (X-CT) in cold rooms (Pinzer and Schneebeli, 2009). Matzl and Schneebeli (2006) also derive snow SSA using infrared photography. Other techniques that are nondestructive enable the rapid retrieval of snow ~~optically equivalent grain size~~ r_e from field measurements. Gergely et al. (2014), for example, demonstrate ~~an accurate~~ a technique to quickly determine the snow optically equivalent diameter from 0.95 µm bi-hemispherical reflectance measurements. Painter et al. (2007) infer snow ~~optical grain radius (r_{eff})~~ r_e from spectral hemispherical directional reflectance factor measurements using a contact probe and a spectrometer.

~~In snowpacks with high temperature gradients the diffusion of vapor causes snow SSA to decrease during the natural process of snow metamorphism (Flanner and Zender, 2006; Wang and Baker, 2014). In isothermal snow, highly faceted snow grains with relatively high SSA and low radii of curvature undergo coarsening in a process driven by the Kelvin effect. Ebner et al. (2015) show that measurements of snow SSA evolution in isothermal snow agree with the isothermal snow metamorphism modeling framework developed by Legagneux et al. (2004) and Legagneux and Domine (2005). These studies express snow SSA~~ While previous studies monitor snow metamorphism in clean snow, in ~~isothermal metamorphism as a function of time t as follows,~~

~~$$\mathrm{SSA} = \mathrm{SSA}_0 \left(\frac{\tau}{\tau + t} \right)^{1/n},$$~~

~~for initial snow SSA_0 at $t = 0$ and adjustable parameters τ~~ situ experimentation of how LAPs affect the snow grain-size feedback diurnally in natural environments is challenging. These challenges can be partly attributed to the limited availability of inexpensive snow SSA measurement devices that can operate quickly in the field, and ~~n. Domine et al. (2009), however, observe increasing snow SSA due to the fragmentation of surface snow grains mobilized by wind.~~

~~Currently, it is still unclear how solar heating of snow by LAI affects possible negative feedbacks relating to temperature gradient metamorphism. The combined net effect of positive and negative feedback mechanisms within snowpacks is unknown and difficult to study in nature because measurement techniques easily disturb the natural snow structure. The question remains whether or not enhanced solar heating from LAI at the surface could slow metamorphism by weakening the temperature gradient and associated vertical flux of vapor. In light of these current unknowns, the purpose of this studyis twofold: One, to investigate the effects of added LAI on snow albedo feedback; and two,~~ to the numerous constraints on being able to reproduce naturally occurring conditions for which LAPs in snow strongly influence the climate system. While the POSSUM is a suitable instrument for this study, here, our first objective is to demonstrate the utility of a new instrument we use to quickly obtain approximate snow ~~SSA. We hypothesize that if we add dust and BC to snow surfaces, then we will induce measurable snow albedo positive~~ *surface* SSA (with LAPs). Our second objective is to investigate the effects of added LAPs on the snow grain-size feedback.

~~To test this hypothesis~~In the following sections, we first describe ~~the design principle~~ a numerical model that simulates multiple scattering in three dimensions to aid the design and calibration of the Near-Infrared Emitting and Reflectance Monitoring Dome (NERD)~~, an instrument that is placed gently onto the snow surface to obtain snow SSA. The NERD~~. Next, we describe the NERD apparatus, which enables multiple 1.30 and 1.55 μm bidirectional reflectance factor (BRF) measurements in just minutes ~~with minimal alteration of~~ while minimally altering the snow structure. To calibrate the NERD with respect to snow SSA, we then compare snow BRFs with X-CT derived SSA and ~~find an exponential relationship between~~ develop an empirical relationship between measured SSA and snow 1.30 μm BRFs. ~~These relationships are also explored using a three dimensional Monte Carlo photon transport model. We then present~~ Finally, we discuss results from our ~~LAI~~ LAP in snow experiments ~~. We discuss these results and their implications.~~ in which we monitored accelerated snow metamorphism. Overall, this study demonstrates the NERD measurement technique and conditions for which ~~snow metamorphism~~ the snow grain-size feedback can be enhanced by the presence of ~~LAI~~LAPs.

2 Instrumentation and Methods

2.1 ~~The Near-Infrared Emitting~~ Monte Carlo Modeling of Multiple Scattering in Snowpack

The Monte Carlo method is applied to numerically simulate three dimensional (3D) light scattering within an idealized snowpack. Gaussian distributions (with 0.085 and ~~Reflectance-Monitoring Dome (~~0.130 μm full width at half-maximums) of photon wavelengths (centered around 1.30 and 1.55 μm) were selected to model light emission by narrow-band infrared light emitting diodes (LEDs). One by one, photons are initiated downward into the snow medium, as demonstrated by Kaempfer et al. (2007), and propagated in optical depth space. Extinction, absorption, and polarization are accounted for following the scattering approach for geometrical optics described by Malinka (2014). Accordingly, random numbers (RN_i) in the interval (0, 1) are generated to determine the photon optical path lengths, l_i, such that

$$l_i = \ln(1/\mathrm{RN}_i) \tag{3}$$

before the first scattering event ($i = 0$) and again after each scattering event i. Absorption (and termination) of a photon can occur during a scattering event if an additionally generated random number (between 0 and 1) is greater than the particle's single scattering albedo. When a photon is scattered, its new direction cosines are determined from an optimized "rejection method" using the particles' scattering matrices (Ramella-Roman et al., 2005).

To calculate snow BRFs, 1,000,000 photons are propagated and traced through modeled snowpack until they are absorbed or exit the medium. The snowpack is modeled as two phase (air and ice) media containing a regular arrangement of suspended homogenous ice particles. Aspherical particle single scattering properties, including the mass absorption cross sections, asymmetry parameters, single scattering albedos, projected areas, volumes, and scattering matrices were calculated by Yang et al. (2013) for randomly oriented droxtals and solid hexagonal columns. For spheres, Mie Theory is applied, but with the analytical Henyey-Greenstein phase function (van de Hulst, 1968) to improve computational efficiency. The subset of shape habits (smooth droxtals and hexagonal columns) from the large dataset provided by Yang et al. (2013) was selected because these shape habits

are purely convex solid ice. Because they are solid convex bodies, their SSAs can be computed from the their projected areas and volumes (Vouk, 1948). Azimuthal mean BRFs are calculated according to the reflectance definitions presented by Dumont et al. (2010) Hudson et al. (2006), and Nicodemus et al. (1977). Accordingly, photon exit angles are grouped into 30 exit zenith angle (θ_r) bins at three degree resolution. Azimuthal (ϕ) mean BRFs are calculated by zenith angle, θ_r, from the total incident photon flux, Φ_i (at a given θ_i), from

$$R(\theta_i;\theta_r) = (2\Phi_i \sin\theta_r \cos\theta_r)^{-1} \int_0^{2\pi} d\Phi_r d\phi, \tag{4}$$

where $d\Phi_r$ represents the reflected photon flux through discrete solid angle bins. In the denominator, the $\cos\theta_r$ factor satisfies Lambert's cosine law while $\sin\theta_r$ accounts for the zenith angular dependence of the azimuthally integrated projected solid angle. Finally, the factor two is necessary to normalize the resulting weighting function $w(\theta_r) = \sin\theta_r \cos\theta_r$, as

$$\int_0^{\pi/2} \sin\theta_r \cos\theta_r d\theta = \frac{1}{2}. \tag{5}$$

Statistical uncertainty was determined by computing BRFs from simulations of Lambertian surfaces and tested using different numbers of photons. Azimuthal averaging reduces the BRFs' dimensionality, so that fewer photons are needed to mitigate Monte Carlo noise. Eq. 4 was initially applied to Monte Carlo simulations of 75 thousand photons reflected by various ideal Lambertian surfaces. At three degree (zenith angular) resolution, 30 and 60 degree BRFs of Lambertian surfaces were simulated accurately to within +/- 2 %. This margin of uncertainty was determined by computing RMS differences between calculated and specified Lambertian reflectances ranging from 0 to 1. Across this range, RMS differences at 30 and 60 degrees were generally less than 0.01. In subsequent test cases, simulating snowpack BRFs with up to 10,000,000 photons did not significantly change results when compared with simulations of 250,000 photons. Ultimately, it was determined that simulations with 1,000,000 photons were appropriate for the remainder of this study.

2.2 Near-Infrared Bidirectional Reflectance Factor Measurements

The NERD ~~)The NERD~~ is designed to measure 1.30 and 1.55 μm BRFs. These wavelengths are selected for snow SSA retrieval due to the strong dependence of snow albedo on ~~snow optical grain size (i. e. sphere equivalent radius).~~ grain size in these parts of the spectrum. Snow spectral albedo is simulated here using the SNICAR model to demonstrate this sensitivity (Fig. 1). While snow spectral albedo is sensitive to snow ~~optical grain size~~ r_e (and thus snow SSA), it is not sensitive to small black carbon concentrations at these wavelengths. Snow SSA can therefore be retrieved using 1.30 μm and 1.55 μm reflectance measurements for snow with small black carbon concentrations.

The design principle is similar to the DUal Frequency Integrating Sphere for Snow SSA measurements (DUFISSS) (Gallet et al., 2009). The NERD also uses 1.30 (1.31 in DUFISSS) and 1.55 μm emitters to illuminate the snow surface from nadir (15 degrees off nadir for 1.55 μm in NERD). The main distinction between the DUFISSS and the NERD is the type of reflectance

measured. Gallet et al. (2009) use an integrating sphere to measure hemispherical reflectance. In the NERD, however, photodiodes are directed toward the illuminated surface in a black dome to measure BRFs, as demonstrated by Arnaud et al. (2011) . The interior of the dome is painted with a flat black paint to increase absorptivity and minimize internal reflections between the dome and snow surface. To test the near-infrared absorptivity of the black pigment, the NERD was used to measure BRFs of a painted black surface. All measured BRFs of the black surface were less than 0.03.

Four infrared light emitting diodes (LEDs) are mounted into ~~a~~ the 17 cm diameter black styrene half-sphere. Two LEDs with peak emission wavelengths of 1.30 µm are mounted at nadir and ten degrees relative to zenith and two LEDs with peak emission wavelengths of 1.55 µm are mounted at 15 degrees off nadir (see Fig. 2). 1.30 µm LEDs have spectral line half widths of ~~85 nm~~ 0.085 µm and half intensity beam angles of ten degrees, while 1.55 µm LEDs have half-maximum bandwidths of ~~130 nm~~ 0.130 µm and 20 degree beam angles. These high powered, narrow beam infrared LEDs ~~are~~ were selected to illuminate a small oval (estimated major axes of 1.5 cm at 1.30 µm and 3.0 cm at 1.55 µm) of the experimental surface to maximize the reflected radiance signal. The reflected radiance signal is measured using four InGaAs photodiodes mounted in two different azimuthal planes (0 and 90 degrees relative to the illumination); two each at 30 and 60 degrees relative to zenith. Photodiodes highly sensitive to light ~~ranging from 800 to 1750 nm~~ with wavelengths ranging from 0.80 to 1.75 µm and relatively large active areas (1 mm) ~~are~~ were selected to maximize sensitivity.

Because the orientation of LEDs and photodiodes are fixed, reflectance factors of surfaces with negligible subsurface scattering can be obtained after calibration using two diffuse reflectance targets ~~in a manner similar to that used by Gallet et al. (2009), Gergely et al. (2014), and Dumont et al. (2010)~~(Gallet et al., 2009; Gergely et al., 2014; Dumont et al., 2010). These Lambertian targets reflect incident light according to Lambert's cosine law and appear equally bright at all viewing angles. By comparing the measured voltage signal from the experimental (snow) surface to that measured from the reflectance targets, two BRFs at both 30 and 60 degree viewing angles are obtained for each light source. While subsurface scattering of visible light in snow is pervasive (Smith et al., 2018), the light penetration in snow near 1.30 and 1.55 µm is at most a couple centimeters due to the strong absorption features in the near-infrared (Kaempfer et al., 2007; Grenfell et al., 1994; Brandt and Warren, 1993). Subsurface scattering is therefore assumed to be minimal and fully contained within each photodiode's field of view. ~~Therefore, this procedure enables simultaneous measurements of multiple snow BRFs at 1.30 and 1.55 µm.~~

To validate NERD reflectance measurement accuracy, precision, and responsiveness, measured BRFs of reflectance standards are recorded after calibration. Ten BRFs (R) for each LED / photodiode viewing zenith angle (θ_i;~~θ_r~~θ_i;θ_r) combination are measured in temperatures ranging from -20 ° to +2 °C. In general, NERD BRFs of the Lambertian reflectance standards are accurate to within +/- 2 %. We quantify instrument precision (2 %) by computing root mean squared (RMS) differences from repeated measurements (see Table 1). Linear regressions quantify the linear response (A) over the reflectance range of 0.41 to 0.95. Response uncertainty ranges from -2 % to +3 % and from +1 % to +3 % at 1.30 and 1.55 ~~µ~~µm, respectively. These test results indicate the NERD's ability to obtain BRFs on smooth reflectance standards with a measurement uncertainty of 1-2 %.

2.3 Snow Specific Surface Area Measurements

2.3.1 ~~Snow samples~~

Surface snow (just the top few centimeters) samples were collected in nature over the span of three years (winters 2015-2017) and transported in coolers to the nearby US Army's Cold Regions Research Engineering Laboratory (CRREL) in Hanover, New Hampshire. Depth hoar samples, however, were instead grown inside the CRREL at -20 °C using a forced temperature gradient. Snow samples are classified based on X-CT results according to Fierz et al. (2009) (Table 2). Snow SSA was derived from X-CT analysis and contact spectroscopy, as described below.

2.3.1 X-ray ~~micro-computed tomography~~ Micro-computed Tomography (X-CT)

To determine snow SSA, X-CT was conducted on a class of six snow samples according to Lieb-Lappen et al. (2017). X-ray (40-45 kV, 177-200 micro-Amps) transmission through cylindrical snow samples was measured at rotation steps of 0.3-0.4 degrees. To limit scan times to 15 minutes, exposure time was set to 340 ms at a cubic voxel resolution of 14.9 µm. Processing software enables SSA calculations from ~~three dimensional~~ 3D morphology results (Pinzer and Schneebeli, 2009).

In some cases, snow samples were scanned several hours or days after snow BRFs were measured. To correct for natural isothermal snow SSA metamorphism while samples were being stored, eq. 2 was applied with t set equal to the total time elapsed between NERD measurements and X-CT scan times and with ~~τ and n~~ $\tau = 721.2$ or 14400 and $n = 2.15$ or 0.32, respectively, inferred from Ebner et al. (2015) depending on the snow sample type. Applying this correction yielded a SSA decrease between 3 and 5 m^2 kg^{-1}.

2.3.2 Contact ~~spectroscopy~~Spectroscopy

Snow SSA was also inferred from optical grain size measurements using contact spectroscopy (Painter et al., 2007). Snow reflectance spectra ~~are~~ were collected using an ASD FieldSpec4 and ~~high-intensity~~ a high intensity contact probe with reference to a Spectralon white reference panel. ~~The effective radius~~ Snow r_e is determined from the normalized area of the absorption feature centered at approximately 1 ~~nm~~ µm using a look up table (Nolin and Dozier, 2000). These measurements were conducted ~~on depth hoar created~~ inside the CRREL in a cold lab only for the depth hoar (DH_2016) and ~~on~~ rounded grains (RG_2015) samples.

2.4 ~~Monte Carlo Modeling of Bidirectional Reflectance Factors~~Light Absorbing Particles in Snow Experiments

~~The Monte Carlo method is applied in this study to numerically simulate light emission by the NERD and the resulting three dimensional light scattering within modeled snow packs. Arrays of photons with wavelengths generated at random using Gaussian distributions are used to mimic the 85 and 130 nm full width at half-maximum spectral emission characteristics of the narrow-band LEDs mounted in the NERD. These LEDs are modeled as photon emitters according to their orientation in the dome. Photons are initiated downward into the snow medium, as demonstrated by Kaempfer et al. (2007), and propagated~~

in optical depth space. Photon particle interactions are determined using random number generators. Photons can either be absorbed or scattered with the probability determined by the particle single scattering albedo. Photons are terminated upon absorption and followed if scattered. When a photon is scattered, its new direction cosines are determined by the particle scattering phase function. 1,000,000 photons per simulation are propagated and followed through the snow medium until they are absorbed or exit the medium. The snow packs are modeled as homogenous matrices of suspended particles with input data containing the particle mass absorption cross section, asymmetry parameter, single scattering albedo, projected area, volume, and scattering matrix. These scattering properties are calculated by Yang et al. (2013) for randomly oriented ice particle shape habits that include droxtals, solid hexagonal columns, and spheres. For spheres, we apply the Henyey-Greenstein phase function

$$P_{\mathrm{HG}}(\cos\theta; g) = \frac{1-g^2}{(1+g^2-2g\cos\theta)^{3/2}},$$

where θ is the scattering angle and g is the relevant asymmetry parameter. We select these subset of shape habits from the larger dataset provided by Yang et al. (2013) because they are purely convex solid ice particles. Because they are convex bodies, their SSAs can be computed from the projected area and volume.

Azimuthal mean BRFs are calculated according to the reflectance definitions presented by Dumont et al. (2010) Hudson et al. (2006) , and Nicodemus et al. (1977). Accordingly, photon exit angles are grouped into 30 exit zenith angle (θ_r) bins at three degree resolution. Azimuthal mean BRFs are calculated by zenith angle θ_r from the total incident photon flux Φ_i by

$$R(\theta_i; \theta_r) = \int_0^{2\pi} \frac{d\Phi_r}{2\sin\theta_r\cos\theta_r\Phi_i} d\phi_r$$

where Φ_r represents the azimuthally integrated photon flux through each θ_r bin. In the denominator, the $\cos\theta_r$ factor satisfies Lambert's cosine law while $\sin\theta_r$ accounts for the zenith angular dependence of the azimuthally integrated projected solid angle. Finally, the factor two is necessary to normalize the resulting weighting function $w(\theta_r) = \sin\theta_r\cos\theta_r$, as

$$\int_0^{\pi/2} \sin\theta_r\cos\theta_r d\theta_r = \frac{1}{2}.$$

Monte Carlo noise is tested by computing BRFs from simulations of Lambertian surfaces. Azimuthal averaging reduces the BRFs' dimensionality, so that fewer photons are needed to mitigate Monte Carlo noise. Equation (5) is applied to Monte Carlo simulations of 75 thousand photons reflected by Lambertian surfaces having reflectances of zero to one. At three degree resolution, 30 and 60 degree BRFs of Lambertian surfaces are simulated accurately to within +/- 2 %. Monte Carlo noise from 75 thousand photons are quantified by computing RMS differences across the full range of Lambertian reflectances. Across this range, RMS differences at 30 and 60 degrees are generally less than 0.01. These results indicate that at least 75 thousand photons are needed to mitigate Monte Carlo noise and sufficiently simulate accurate BRFs for Lambertian surfaces at three degree resolution. In a few additional test cases, simulating snow BRFs with up to 10,000,000 photons did not significantly change results when compared with simulations of 250,000 photons.

2.5 ~~LAI in Snow Experimental Procedure~~

Snow BRFs and SSA were measured throughout the day in the following dust and BC in snow experiments. Sand particles and hydrophobic BC were sifted multiple times with a salt shaker (with holes of roughly 1 mm diameter) to filter out larger particles. The filtered ~~LAI~~ LAPs were then deposited onto experimental snow plots in an open field in Hanover, New Hampshire on February 10 and February 16, 2017 shortly after fresh snowfall events. For each experiment, one square meter plots of snow were designated as natural (control) or contaminated (experimental). Snow BRFs and SSA ~~are~~ were obtained using the NERD and from X-CT analysis, respectively. For each set of NERD measurements, 30 degree and 60 degree BRFs are both recorded four times. BRFs ~~are~~ were measured over two different locations within the experimental plot using two photodiodes at each viewing angle (30 and 60 degrees).

2.4.1 Cloudy Sky with Diffuse Ambient Lighting (February 10~~experiment (cloudy sky / diffuse ambient lighting,~~ 2017)

Early on February 10, experimental plots were loaded with BC until visible darkening was apparent. Snow BRFs were measured shortly after 00:00, 03:00, 06:00 Eastern Standard Time (EST) (during the night), and then periodically throughout the day. Because these plots were well shaded by tall trees, these measurements were used to monitor snow metamorphism without the influence of direct solar illumination. Furthermore, mostly cloudy conditions on February 10 ~~diffused incoming~~ obscured direct solar radiation so that ambient lighting was ~~nearly isotropic~~diffuse.

2.4.2 Clear Sky with Direct Solar Irradiance (February 17~~experiment (clear sky / direct solar heating~~, 2017)

On February 17, just a pinch (< 1 g) of BC and ~~30g~~ 30 g of sand were deposited ~~on separate experimental~~ (quasi-) uniformly over separate one square meter plots. These ~~surface~~ experimental deposition fluxes were selected to mimic ~~extreme LAI deposition~~ the most extreme LAP loading events observed by Skiles and Painter (2017) in the San Juan Mountains in Colorado. As in the previous experiment, snow BRFs were measured periodically throughout the day, however, all snow plots were in full view of the clear sky to maximize incident direct solar irradiance.

3 Results and Discussion

3.1 ~~Monte Carlo modeling~~Near-Infrared Reflectance Calculations for Regular Homogenous Ice Particles

To validate the Monte Carlo model for snow applications, we simulated 1.30 and 1.55 µm narrow band black-sky albedo ~~was calculated and compared to the SNICAR model for snow Re~~ for snow r_e ranging from 36 to 327 µm (SSA = 80 to 10 m^2kg^{-1}) ~~(see~~ and compared results with the SNICAR model (Fig. 3~~, left~~). As expected, ~~Monte Carlo results from snow modeled as spherical ice particles were consistent with narrow-band albedo calculations from Flanner et al. (2007). These results show~~ results from Monte Carlo simulations yield slightly higher hemispheric reflectances for droxtals (for all SSA) and solid hexagonal columns (for SSA $>$ 40 m^2kg^{-1}) than ~~those calculated from equal SSA~~ for spheres and from the

SNICAR model (Dang et al., 2016). For all particle sizes, Monte Carlo simulations using spherical ice particles generated nearly identical narrow-band albedo values compared to those from Flanner et al. (2007). These results are also similar to the numerical modeling results from Picard et al. (2009) and the analytical solutions from Kokhanovsky and Zege (2004), though for different particle shapes. ~~We hypothesize that the variations in these albedo calculations, and also BRFs, across particle shapesare inversely related to the particles' asymmetry parameters.~~

To inform on our choice of a snow BRF to SSA calibration function, ~~Monte Carlo simulated snow BRFs are calculated for various (homogeneous)~~ we calculated BRFs from eq. 4 for various particle SSA ranging from 10 to 80 m^2kg^{-1} ~~and plotted against measurement data in Fig. 4.~~ (Fig. 4, line graphs). Generally, we found exponential (linear) relationships between 1.30 (1.55) µm BRFs and ~~snow SSA for spheres, droxtals, and solid hexagonal columns. 1.3~~ particle SSAs. Modeled 1.30 µm ~~BRF calculations~~ BRFs are slightly higher at 30 degrees than at 60 degrees for particle SSA > 30 m^2kg^{-1}. ~~At 1.30 µm, measured 30 degree snow BRFs for varying snow SSA fall within the envelope of modeled BRFs for all three shape habits. These modeling results are in closest agreement with measurements at 30 degrees viewing for 1.30 µm. At 1.55 µm, measured BRFs are larger than predicted from modeling across all SSA.~~ For a given particle size, a different shape habit can yield a change in BRFs of as much as 0.1. Monte Carlo modeling results yield the highest reflectances for droxtals and the lowest reflectances for spheres.

3.2 ~~NERD~~ Relating Snow ~~SSA Calibration~~Specific Surface Area to Near-Infrared Bidirectional Reflectance Factors

To calibrate the NERD for snow SSA retrieval, we ~~compare~~ compared X-CT derived snow SSA with NERD snow BRF measurements (~~see~~ Fig. 4). In general, measured snow BRFs are directly related to snow SSA. At 1.30 µm BRFs range from just under 0.2 (for low SSA) to as high as 0.7 (for high SSA) and are slightly higher at 60 degrees than at 30 degrees. We ~~observe~~ observed 1.55 µm snow BRFs close to 0 (for low SSA) and as high as 0.2 (for high SSA). We ~~observe~~ recorded the highest 1.55 µm snow BRFs at 60 degrees for fresh snow (needles). At 1.30 µm, measured 30 degree snow BRFs for varying snow SSA fall within the envelope of Monte Carlo modeled BRFs for all three shape habits (Fig. 4, top left). Modeling results are in closest agreement with measurements at 30 degrees viewing for 1.30 µm. At 1.55 µm, measured BRFs are larger than predicted from modeling across all SSA.

These results ~~show considerable spread~~ demonstrate a considerable spread of BRFs in measurements, across snow samples~~in BRF measurements and across shape habits in Monte Carlo calculations at both wavelengths and at both~~ , and in modeling, across shape habit, for both 1.30 and 1.55 µm and for both 30 and 60 degree viewing angles. The spread in measurements, in particular, indicates a considerable uncertainty in the ability to retrieve snow SSA from ~~NERD~~ measured BRFs. While the 1.30 µm, 30 degree viewing zenith angle BRF combination most closely agrees with modeled BRFs, ~~a similar margin of error at~~ the 60 degree viewing zenith angle can provide a second estimate of snow SSA. Reporting two snow SSA values using both view angles can provide an estimate of the variability in SSA retrieval resulting from the ~~angular dependence~~ anisotropy of the snow ~~BRDF~~ bidirectional reflectance distribution function in the near-infrared ~~. Monte Carlo 30 degree BRFs are larger than 60 degree (viewing; zenith) BRFs. These results are consistent with those from Kaempfer et al. (2007), but at 900 nm.~~ (Dumont et al., 2010).

Our finding of the exponential relationships between snow SSA and 1.30 μm BRFs is consistent with results from previous studies (Picard et al., 2009; Gallet et al., 2009). Gallet et al. (2009) also identify a linear relationship between 1.55 μm reflectance and snow SSA and use the longer wavelength in their DUFISSS to obtain measurements of high snow SSA ($>$ 60 m^2kg^{-1}). In this study, however, nearly all snow samples are lower than this threshold. ~~A possible follow on study would include snow of higher SSA to determine the utility of 1.55 μm snow BRFs in measuring fresh snow of extremely high SSA particularly common in the extremely cold Arctic and Antarctic environments and observed by Legagneux et al. (2002) and Libois et al. (2015).~~

~~Snow BRFs~~ Measured snow BRFs at 1.55 μm ~~observed by the NERD~~ are higher than both hemispherical reflectance measurements by Gallet et al. (2009) and ~~those predicted from Monte Carlo modeling. NERD LEDs~~ Monte Carlo calculations. This discrepancy might be explained by the NERD LEDs, which have full width at ~~half maximums of 130 nm~~ half-maximums (FWHM) of 0.130 μm and emit non-negligible light at ~~wavelengths much shorter , toward the near-infrared. We hypothesize that higher than expected measured 1.55~~ shorter wavelengths. Supplementary SNICAR and albedo calculations using a broadened FWHM of 0.260 μ~~m BRFs are caused by reflected light at shorter wavelengths. Additional SNICAR modeling results and Monte Carlo simulations~~ m support this hypothesis~~(see~~ , where values closer to the measured 1.55 μm BRFs are reproduced (Fig. 3, right).

In light of these empirical and numerical results, we propose the following general exponential form relating 1.30 μm snow BRFs to SSA, such that

$$\mathrm{SSA} = \alpha \exp(R_{1.30}) + \beta \tag{6}$$

for 1.30 μm snow BRF $R_{1.30}$. Using least squares regression analysis, we ~~compute parameters~~ estimate "best fit" values for α and β for both 30 and 60 degree viewing zenith angles (see Fig. 5).

Ideally, an empirically derived calibration function would include SSA measurements from multiple methods to mitigate uncertainties associated with collection methods needed for X-CT analysis. Such collection methods can easily change the snow microphysical characteristics and lead to biases in the X-CT derived SSA. As a preliminary validation of eq. 6, we compare snow SSA results to SSA derived from snow ~~optical effective radii~~ r_e measurements conducted using contact spectroscopy in Fig. 5. Encouragingly, two out of three measurements fall within the bounds of the standard error of the regression. ~~As expected, contact~~ Contact spectroscopy snow SSA values are consistently higher than those calculated from X-CT analysis and ~~therefore eq.~~ are also higher than those determined by eq. 6. ~~Because contact spectroscopy measurements typically yield higher SSA values than those derived from other optical methods, these comparisons, though preliminary , offer some initial validation~~ This comparison provides a preliminary assessment of the NERD snow ~~SSA calibration~~BRF to SSA calibration function.

Hereafter, we apply eq. 6 in the following ~~LAI~~ LAP in snow experiments to estimate hourly snow SSA from measured snow BRFs. Because the remainder of this study is concerned with relatively large changes in SSA, approximate SSA retrieval using the NERD ~~are sufficient~~ is useful to quantitatively assess ~~snow metamorphism in the presence of LAI~~how added LAPs affect snow grain-size feedback and snow metamorphism.

3.3 ~~LAI enhanced snow metamorphism~~Light Absorbing Particles' Effect on Snow Metamorphism

First, to monitor snow metamorphism without solar heating, during the early morning (night) hours on February 10, we ~~deposit~~ deposited BC onto an experimental plot after the previous day's snow fall. Surface temperatures ranged from -14 to -9 °C. We observed low to moderate wind speeds from the early morning hours through the afternoon with partly to mostly cloudy conditions during the day. 1.30 µm snow BRF measurements conducted shortly after BC application indicate a direct darkening of 0.03 at 30 degrees viewing and 0.05 at 60 degrees viewing. While these decreased BRF values are considerable, this experiment contained heavily contaminated snow with a high BC concentration unlikely to occur in nature. Despite the high BC concentration, BRFs measured at 1.30 (1.55) µm remained within 0.5 and 0.6 (0.1 and 0.2) throughout the day in both contaminated and natural snow (see Fig. 6). X-CT analysis showed small differences in morning (49 m^2kg^{-1}) and afternoon (48 m^2kg^{-1}) snow SSA. Our results ~~from this experiment~~ indicate that heavy BC loading had little to no effect on snow metamorphism during the 16 hour experiment without direct solar irradiance.

Second, to monitor snow metamorphism occurring after forced large BC and dust deposition events under direct solar illumination, on February 17, we set up a similar experiment in full view of the sun. Surface temperatures ranged from -4 to +2 °C. We observed minimal wind speeds and cloud cover resulting in calm, clear sky conditions. BRF measurements conducted shortly after LAP application indicate minimal direct darkening at 1.30 µm and possibly a small brightening effect by dust at 1.55 µm. In natural snow, 1.30 µm BRFs remained close to 0.5 throughout the day, with the lowest values (0.49) recorded in the afternoon (13:00 EST) and the highest values (0.55) recorded in the morning (08:00 EST) and evening (17:00 EST). 1.55 µm BRFs remained just above 0.1. In the dust loaded plot, snow 1.30 (1.55) µm BRFs decreased rapidly from above 0.5 (0.1) before 10:~~00am~~ 00 to to below 0.3 (0.05) by ~~1:00pm~~ 13:00 EST. We found less extreme metamorphism in the lightly contaminated snow with added BC, as BRF measurements decreased from above 0.5 (0.1) to below 0.45 (0.1). 1.30 µm snow BRFs slightly increased thereafter (from 13:00 to 17:00 EST) in both natural and contaminated snow (see Fig. 7). Snow SSA also decreased throughout the day. From X-CT analysis, we found morning snow SSA to be about 50 m^2kg^{-1}, which thereafter decreased to 41, 23, and 18 m^2kg^{-1} in natural, BC loaded, and dust loaded snow, respectively. NERD derived snow SSA appears to be biased low in the afternoon dust loaded plot. This bias might be an indication of the presence of liquid water that was also visible to the naked eye. X-CT scans performed on this snow sample are representative of refrozen snow and do not conform to the isothermal snow SSA correction (eq. 2) applied to snow samples scanned several hours after collection. In BC loaded plots, we observed a large spatial heterogeneity in measurements, indicating that small BC deposition has a powerful localized effect on snow metamorphism.

These results suggest that ~~realistic LAI~~ extreme LAP deposition can accelerate snow metamorphism. The primary cause of this accelerated process is enhanced absorption of solar radiation by ~~LAI~~LAP. Surprisingly, added BC had little to no effect on snow metamorphism during cloudy conditions. ~~One possible explanation of this surprising result is that adding BC to snow only initiated melting during clear sky conditions.~~ In the clear sky experiments, ~~LAI~~ LAP enhanced solar absorption at the surface which warmed the snowpack. As the snow surface began to melt, near-infrared reflectance decreased rapidly. Rapidly

decreasing near-infrared reflectance is indicative of either the accumulation of liquid water from melting snow or decreasing snow surface SSA.

Accelerated snow metamorphism by dust loading is consistent with the findings of Skiles and Painter (2017). The indirect effect of ~~LAI~~ LAP on snow is also demonstrated by Hadley and Kirchstetter (2012), where the albedo reduction due to the presence of BC in snow is amplified in snow of lower SSA. This enhancement of snow albedo reduction is another source of instability in the ~~snow pack~~ snowpack that increases the strength of ~~snow internal albedo~~ the snow grain-size feedback. Typical BC deposition events are very small, however, so it is difficult to reproduce natural BC concentrations when adding any BC to a one square meter plot.

4 Conclusions

~~Taken together, these results indicate that LAI deposition can accelerate snow metamorphism and enhance positive snow albedo feedback , especially~~ LAPs in snow accelerated snow metamorphism and enhanced positive grain-size feedback during cloud free, calm weather conditions when surface air temperatures ~~are~~ were near 0°C. To ~~obtain quick, repeatable measurements of snow SSA without destroying samples,~~ observe this effect, we engineered an instrument (i.e., the NERD) that measures 1.30 and 1.55 µm ~~BRFs of snow~~ snow BRFs without destroying snow samples. We evaluated ~~NERD~~ the NERD's accuracy, precision, and responsiveness by testing with idealized Lambertian surfaces before obtaining snow BRFs. Notwithstanding the limitations associated with retrieving precise snow SSA from BRFs, we proposed an analytical calibration function relating snow SSA to 1.30 µm BRFs. Our results lead to the conclusion that the NERD can provide estimates of snow SSA to within +/- 10 m^2kg^{-1}.

The NERD will serve to further study the effects of ~~LAI~~ LAPs on snow metamorphism and to explore the spatial heterogeneity of snow SSA. Because it can also operate quickly, NERD measurements can complement satellite borne observations during narrow sampling windows. To fulfill these pursuits, however, a more comprehensive snow SSA measurement validation is needed ~~. Additional~~ to fully characterize snow SSA measurements by the NERD technique. This would include additional independent measurement methods ~~that include~~ on snow samples with a larger snow SSA span from a variety of environmental conditions and further experimentation into the small scale effects on ~~NERD~~ snow BRF measurements~~are needed to fully justify the NERD as an accurate snow SSA measurement technique~~. Further investigation ~~into the micro-physical limitations and~~ of the natural variability of snow near the surface and the related quantitative uncertainties associated with the ~~precise~~ retrieval of snow SSA from ~~near-infrared BRF measurements is~~ NERD measurements will be the subject of a ~~follow-on study.~~ follow on study. Such a study will also include snow of higher SSA to determine the utility of 1.55 µm snow BRFs in measuring fresh snow of extremely high SSA, as demonstrated by Gallet et al. (2009). This would help expand the utility of the NERD measurement technique for future Arctic and Antarctic campaigns, building on the polar studies conducted by Legagneux et al. (2002) and Libois et al. (2015).

Code and data availability. Plot data referenced in this manuscript and associated Python scripts used to generate figures are made available via the University of Michigan's Deep Blue data repository (Schneider and Flanner, 2018).

Appendix A: NERD Photodiode Current Amplifiers

To detect reflected radiance signals, photodiodes are reverse biased to induce currents linearly related to the amount of light incident on its active region. Because these light signals are reflected from the experimental surface, the currents induced by the photodiodes are very small (nano- to micro-Amps). To measure the small currents, the photodiodes are connected to transimpedance amplifiers. The transimpedance amplifier circuits convert and amplify the small photodiode currents into measurable voltage signals.

Two NERDs are engineered with different photodiode current amplifications. Photodiode current amplification is determined by the feedback resistance in the transimpedance amplifier circuits. Active low pass filters are applied between the amplifier and the analog-to-digital converter (ADC) to reduce noise. This filter is designed to have a time constant of less than 0.5 seconds to achieve balance between adequate noise reduction and speed.

Competing interests. Mark Flanner is currently an editor for *The Cryosphere*. We are not aware of any other competing interests associated with the publication of this manuscript.

Acknowledgements. This work is funded, in part, by the National Science Foundation, grant number ARC-1253154.

The authors would like to thank their colleagues at the Cold Regions Research and Engineering Laboratory (CRREL) in Hanover, New Hampshire for ~~their~~ generous support. In particular, thanks to Zoe Courville and John Fegyveresi for their hospitality and guidance navigating the facilities at CRREL. We also thank Ross Lieblappen for sharing his micro-computed tomography expertise through providing a thorough tutorial for running and analyzing snow scans.

The authors are thankful for reviews from three referees (including Marie Dumont). These detailed reviews were helpful in reorganizing the manuscript and improving the presentation of the key results.

References

Arnaud, L., Picard, G., Champollion, N., Domine, F., Gallet, J., Lefebvre, E., Fily, M., and Barnola, J.: Measurement of vertical profiles of snow specific surface area with a 1 cm resolution using infrared reflectance: instrument description and validation, Journal of Glaciology, 57, 17–29, https://doi.org/10.3189/002214311795306664, https://www.cambridge.org/core/product/identifier/S0022143000204607/type/journal_article, 2011.

Bond, T. C., Doherty, S. J., Fahey, D. W., Forster, P. M., Berntsen, T., DeAngelo, B. J., Flanner, M. G., Ghan, S., Kärcher, B., Koch, D., Kinne, S., Kondo, Y., Quinn, P. K., Sarofim, M. C., Schultz, M. G., Schulz, M., Venkataraman, C., Zhang, H., Zhang, S., Bellouin, N., Guttikunda, S. K., Hopke, P. K., Jacobson, M. Z., Kaiser, J. W., Klimont, Z., Lohmann, U., Schwarz, J. P., Shindell, D., Storelvmo, T., Warren, S. G., and Zender, C. S.: Bounding the role of black carbon in the climate system: A scientific assessment: BLACK CARBON IN THE CLIMATE SYSTEM, Journal of Geophysical Research: Atmospheres, 118, 5380–5552, https://doi.org/10.1002/jgrd.50171, http://doi.wiley.com/10.1002/jgrd.50171, 2013.

Brandt, R. E. and Warren, S. G.: Solar-heating rates and temperature profiles in Antarctic snow and ice, Journal of Glaciology, 39, 99–110, https://doi.org/10.3189/S0022143000015756, https://www.cambridge.org/core/product/identifier/S0022143000015756/type/journal_article, 1993.

Dang, C., Fu, Q., and Warren, S. G.: Effect of Snow Grain Shape on Snow Albedo, Journal of the Atmospheric Sciences, 73, 3573–3583, https://doi.org/10.1175/JAS-D-15-0276.1, http://journals.ametsoc.org/doi/10.1175/JAS-D-15-0276.1, 2016.

Domine, F., Salvatori, R., Legagneux, L., Salzano, R., Fily, M., and Casacchia, R.: Correlation between the specific surface area and the short wave infrared (SWIR) reflectance of snow, Cold Regions Science and Technology, 46, 60–68, https://doi.org/10.1016/j.coldregions.2006.06.002, http://linkinghub.elsevier.com/retrieve/pii/S0165232X06000735, 2006.

Domine, F., Taillandier, A.-S., Cabanes, A., Douglas, T. A., and Sturm, M.: Three examples where the specific surface area of snow increased over time, The Cryosphere, 3, 31–39, https://doi.org/10.5194/tc-3-31-2009, http://www.the-cryosphere.net/3/31/2009/, 2009.

Dumont, M., Brissaud, O., Picard, G., Schmitt, B., Gallet, J.-C., and Arnaud, Y.: High-accuracy measurements of snow Bidirectional Reflectance Distribution Function at visible and NIR wavelengths – comparison with modelling results, Atmospheric Chemistry and Physics, 10, 2507–2520, https://doi.org/10.5194/acp-10-2507-2010, http://www.atmos-chem-phys.net/10/2507/2010/, 2010.

Ebner, P. P., Schneebeli, M., and Steinfeld, A.: Tomography-based monitoring of isothermal snow metamorphism under advective conditions, The Cryosphere, 9, 1363–1371, https://doi.org/10.5194/tc-9-1363-2015, https://www.the-cryosphere.net/9/1363/2015/, 2015.

Fierz, C., Armstrong, R., Durand, Y., Etchevers, P., Greene, E., McClung, D., Nishimura, K., Satyawali, P., and Sokratov, S.: The International Classification for Seasonal Snow on the Ground, 2009.

Flanner, M. G. and Zender, C. S.: Linking snowpack microphysics and albedo evolution, Journal of Geophysical Research, 111, https://doi.org/10.1029/2005JD006834, http://doi.wiley.com/10.1029/2005JD006834, 2006.

Flanner, M. G., Zender, C. S., Randerson, J. T., and Rasch, P. J.: Present-day climate forcing and response from black carbon in snow, Journal of Geophysical Research, 112, https://doi.org/10.1029/2006JD008003, http://doi.wiley.com/10.1029/2006JD008003, 2007.

Flanner, M. G., Zender, C. S., Hess, P. G., Mahowald, N. M., Painter, T. H., Ramanathan, V., and Rasch, P. J.: Springtime warming and reduced snow cover from carbonaceous particles, Atmospheric Chemistry and Physics, 9, 2481–2497, https://doi.org/10.5194/acp-9-2481-2009, http://www.atmos-chem-phys.net/9/2481/2009/, 2009.

Gallet, J.-C., Domine, F., Zender, C. S., and Picard, G.: Measurement of the specific surface area of snow using infrared reflectance in an integrating sphere at 1310 and 1550 nm, The Cryosphere, 3, 167–182, https://doi.org/10.5194/tc-3-167-2009, http://www.the-cryosphere.net/3/167/2009/, 2009.

Gallet, J.-C., Domine, F., and Dumont, M.: Measuring the specific surface area of wet snow using 1310 nm reflectance, The Cryosphere, 8, 1139–1148, https://doi.org/10.5194/tc-8-1139-2014, https://www.the-cryosphere.net/8/1139/2014/, 2014.

Gergely, M., Wolfsperger, F., and Schneebeli, M.: Simulation and Validation of the InfraSnow: An Instrument to Measure Snow Optically Equivalent Grain Size, IEEE Transactions on Geoscience and Remote Sensing, 52, 4236–4247, https://doi.org/10.1109/TGRS.2013.2280502, http://ieeexplore.ieee.org/document/6606890/, 2014.

Grenfell, T. C., Warren, S. G., and Mullen, P. C.: Reflection of solar radiation by the Antarctic snow surface at ultraviolet, visible, and near-infrared wavelengths, Journal of Geophysical Research, 99, 18 669, https://doi.org/10.1029/94JD01484, http://doi.wiley.com/10.1029/94JD01484, 1994.

Hadley, O. L. and Kirchstetter, T. W.: Black-carbon reduction of snow albedo, Nature Climate Change, 2, 437–440, https://doi.org/10.1038/nclimate1433, http://www.nature.com/articles/nclimate1433, 2012.

Hagenmuller, P., Matzl, M., Chambon, G., and Schneebeli, M.: Sensitivity of snow density and specific surface area measured by microtomography to different image processing algorithms, The Cryosphere, 10, 1039–1054, https://doi.org/10.5194/tc-10-1039-2016, https://www.the-cryosphere.net/10/1039/2016/, 2016.

Hall, A.: The Role of Surface Albedo Feedback in Climate, Journal of Climate, 17, 1550–1568, https://doi.org/10.1175/1520-0442(2004)017<1550:TROSAF>2.0.CO;2, http://journals.ametsoc.org/doi/abs/10.1175/1520-0442%282004%29017%3C1550%3ATROSAF%3E2.0.CO%3B2, 2004.

Hudson, S. R., Warren, S. G., Brandt, R. E., Grenfell, T. C., and Six, D.: Spectral bidirectional reflectance of Antarctic snow: Measurements and parameterization, Journal of Geophysical Research, 111, https://doi.org/10.1029/2006JD007290, http://doi.wiley.com/10.1029/2006JD007290, 2006.

Kaempfer, T. U., Hopkins, M. A., and Perovich, D. K.: A three-dimensional microstructure-based photon-tracking model of radiative transfer in snow, Journal of Geophysical Research, 112, https://doi.org/10.1029/2006JD008239, http://doi.wiley.com/10.1029/2006JD008239, 2007.

Kokhanovsky, A. A. and Zege, E. P.: Scattering optics of snow, Applied Optics, 43, 1589, https://doi.org/10.1364/AO.43.001589, https://www.osapublishing.org/abstract.cfm?URI=ao-43-7-1589, 2004.

Legagneux, L. and Domine, F.: A mean field model of the decrease of the specific surface area of dry snow during isothermal metamorphism: MODEL OF SNOW SURFACE AREA DECREASE, Journal of Geophysical Research: Earth Surface, 110, n/a–n/a, https://doi.org/10.1029/2004JF000181, http://doi.wiley.com/10.1029/2004JF000181, 2005.

Legagneux, L., Cabanes, A., and Dominé, F.: Measurement of the specific surface area of 176 snow samples using methane adsorption at 77 K: MEASUREMENT USING METHANE ADSORPTION AT 77 K, Journal of Geophysical Research: Atmospheres, 107, ACH 5–1–ACH 5–15, https://doi.org/10.1029/2001JD001016, http://doi.wiley.com/10.1029/2001JD001016, 2002.

Legagneux, L., Taillandier, A.-S., and Domine, F.: Grain growth theories and the isothermal evolution of the specific surface area of snow, Journal of Applied Physics, 95, 6175–6184, https://doi.org/10.1063/1.1710718, http://aip.scitation.org/doi/10.1063/1.1710718, 2004.

Libois, Q., Picard, G., Arnaud, L., Dumont, M., Lafaysse, M., Morin, S., and Lefebvre, E.: Summertime evolution of snow specific surface area close to the surface on the Antarctic Plateau, The Cryosphere, 9, 2383–2398, https://doi.org/10.5194/tc-9-2383-2015, https://www.the-cryosphere.net/9/2383/2015/, 2015.

Lieb-Lappen, R., Golden, E., and Obbard, R.: Metrics for interpreting the microstructure of sea ice using X-ray micro-computed tomography, Cold Regions Science and Technology, 138, 24 – 35, https://doi.org/https://doi.org/10.1016/j.coldregions.2017.03.001, http://www.sciencedirect.com/science/article/pii/S0165232X17301040, 2017.

Malinka, A. V.: Light scattering in porous materials: Geometrical optics and stereological approach, Journal of Quantitative Spectroscopy and Radiative Transfer, 141, 14–23, https://doi.org/10.1016/j.jqsrt.2014.02.022, https://linkinghub.elsevier.com/retrieve/pii/S002240731400079X, 2014.

Matzl, M. and Schneebeli, M.: Measuring specific surface area of snow by near-infrared photography, Journal of Glaciology, 52, 558–564, https://doi.org/10.3189/172756506781828412, https://www.cambridge.org/core/product/identifier/S0022143000209301/type/journal_article, 2006.

Nicodemus, F., Richmond, J., Hsia, J., Ginsberg, I., and Limperis, T.: Geometrical considerations and nomenclature for reflectance, National Bureau of Standards, 1977.

Nolin, A. W. and Dozier, J.: A Hyperspectral Method for Remotely Sensing the Grain Size of Snow, Remote Sensing of Environment, 74, 207 – 216, https://doi.org/https://doi.org/10.1016/S0034-4257(00)00111-5, http://www.sciencedirect.com/science/article/pii/S0034425700001115, 2000.

Painter, T. H., Molotch, N. P., Cassidy, M., Flanner, M., and Steffen, K.: Contact spectroscopy for determination of stratigraphy of snow optical grain size, Journal of Glaciology, 53, 121–127, https://doi.org/10.3189/172756507781833947, https://www.cambridge.org/core/product/identifier/S0022143000201846/type/journal_article, 2007.

Picard, G., Arnaud, L., Domine, F., and Fily, M.: Determining snow specific surface area from near-infrared reflectance measurements: Numerical study of the influence of grain shape, Cold Regions Science and Technology, 56, 10–17, https://doi.org/10.1016/j.coldregions.2008.10.001, http://linkinghub.elsevier.com/retrieve/pii/S0165232X08001602, 2009.

Pinzer, B. R. and Schneebeli, M.: Snow metamorphism under alternating temperature gradients: Morphology and recrystallization in surface snow, Geophysical Research Letters, 36, https://doi.org/10.1029/2009GL039618, http://doi.wiley.com/10.1029/2009GL039618, 2009.

Qian, Y., Yasunari, T. J., Doherty, S. J., Flanner, M. G., Lau, W. K. M., Ming, J., Wang, H., Wang, M., Warren, S. G., and Zhang, R.: Light-absorbing particles in snow and ice: Measurement and modeling of climatic and hydrological impact, Advances in Atmospheric Sciences, 32, 64–91, https://doi.org/10.1007/s00376-014-0010-0, http://link.springer.com/10.1007/s00376-014-0010-0, 2015.

Qu, X. and Hall, A.: What Controls the Strength of Snow-Albedo Feedback?, Journal of Climate, 20, 3971–3981, https://doi.org/10.1175/JCLI4186.1, http://journals.ametsoc.org/doi/abs/10.1175/JCLI4186.1, 2007.

Ramella-Roman, J. C., Prahl, S. A., and Jacques, S. L.: Three Monte Carlo programs of polarized light transport into scattering media: part I, Optics Express, 13, 4420, https://doi.org/10.1364/OPEX.13.004420, https://www.osapublishing.org/oe/abstract.cfm?uri=oe-13-12-4420, 2005.

Schneider, A. and Flanner, M.: Supporting data for the Near-Infrared Emitting and Reflectance-Monitoring Dome, https://doi.org/10.7302/Z23F4MVC, http://deepblue.lib.umich.edu/data/concern/generic_works/79407x76d, type: dataset, 2018.

Skiles, S. M. and Painter, T.: Daily evolution in dust and black carbon content, snow grain size, and snow albedo during snowmelt, Rocky Mountains, Colorado, Journal of Glaciology, 63, 118–132, https://doi.org/10.1017/jog.2016.125, https://www.cambridge.org/core/product/identifier/S0022143016001258/type/journal_article, 2017.

Skiles, S. M., Flanner, M., Cook, J. M., Dumont, M., and Painter, T. H.: Radiative forcing by light-absorbing particles in snow, Nature Climate Change, 8, 964–971, https://doi.org/10.1038/s41558-018-0296-5, http://www.nature.com/articles/s41558-018-0296-5, 2018.

Smith, B. E., Gardner, A., Schneider, A., and Flanner, M.: Modeling biases in laser-altimetry measurements caused by scattering of green light in snow, Remote Sensing of Environment, 215, 398–410, https://doi.org/10.1016/j.rse.2018.06.012, https://linkinghub.elsevier.com/retrieve/pii/S0034425718302918, 2018.

van de Hulst, H.: Asymptotic fitting, a method for solving anisotropic transfer problems in thick layers, Journal of Computational Physics, 3, 291–306, https://doi.org/10.1016/0021-9991(68)90023-5, https://linkinghub.elsevier.com/retrieve/pii/0021999168900235, 1968.

Vouk, V.: Projected Area of Convex Bodies, Nature, 162, 330–331, https://doi.org/10.1038/162330a0, http://www.nature.com/articles/162330a0, 1948.

Wang, X. and Baker, I.: Evolution of the specific surface area of snow during high-temperature gradient metamorphism, Journal of Geophysical Research: Atmospheres, 119, 13,690–13,703, https://doi.org/10.1002/2014JD022131, http://doi.wiley.com/10.1002/2014JD022131, 2014.

Warren, S. G. and Wiscombe, W. J.: A Model for the Spectral Albedo of Snow. II: Snow Containing Atmospheric Aerosols, Journal of the Atmospheric Sciences, 37, 2734–2745, https://doi.org/10.1175/1520-0469(1980)037<2734:AMFTSA>2.0.CO;2, http://journals.ametsoc.org/doi/abs/10.1175/1520-0469%281980%29037%3C2734%3AAMFTSA%3E2.0.CO%3B2, 1980.

Wiscombe, W. J. and Warren, S. G.: A Model for the Spectral Albedo of Snow. I: Pure Snow, Journal of the Atmospheric Sciences, 37, 2712–2733, https://doi.org/10.1175/1520-0469(1980)037<2712:AMFTSA>2.0.CO;2, http://journals.ametsoc.org/doi/abs/10.1175/1520-0469%281980%29037%3C2712%3AAMFTSA%3E2.0.CO%3B2, 1980.

Yang, P., Bi, L., Baum, B. A., Liou, K.-N., Kattawar, G. W., Mishchenko, M. I., and Cole, B.: Spectrally Consistent Scattering, Absorption, and Polarization Properties of Atmospheric Ice Crystals at Wavelengths from 0.2 to 100 μm, Journal of the Atmospheric Sciences, 70, 330–347, https://doi.org/10.1175/JAS-D-12-039.1, http://journals.ametsoc.org/doi/abs/10.1175/JAS-D-12-039.1, 2013.

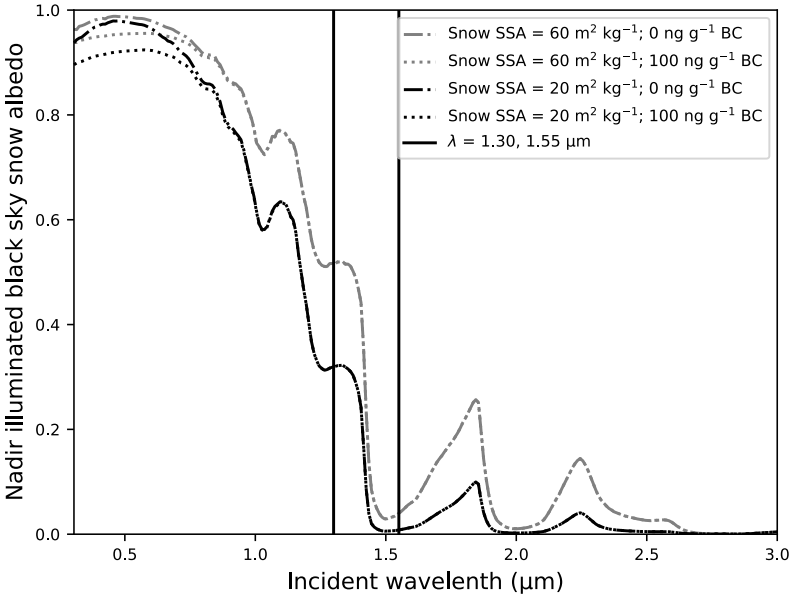

Figure 1. Black sky spectral snow albedo under nadir illumination. Snow albedo is simulated by the Snow, Ice, and Aerosol Radiation (SNICAR) model (Flanner et al., 2007). Dashed-dotted curves represent clean snow of medium-high SSA (60 m^2 kg^{-1}, gray) and medium-low SSA (20 m^2 kg^{-1}, black) to show the dependence of snow albedo on snow SSA. Dotted curves represent contaminated snow with uncoated black carbon (BC) particulate concentrations of 100 ng g^{-1}.

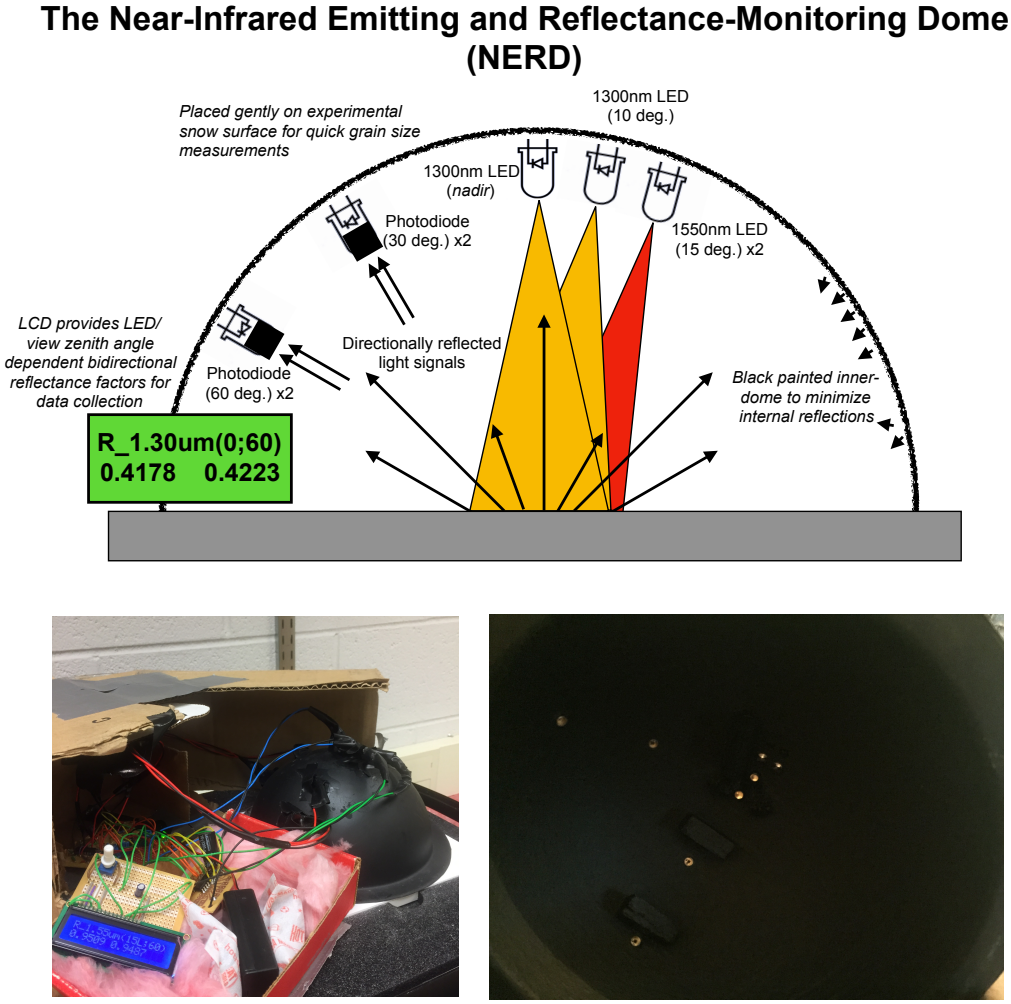

Figure 2. Near-Infrared Emitting and Reflectance-Monitoring Dome (NERD) schematic (top) and photographs (bottom). The photograph on the bottom right shows the (radial) placement of photodiodes and LEDs (toward the center) within the dome.

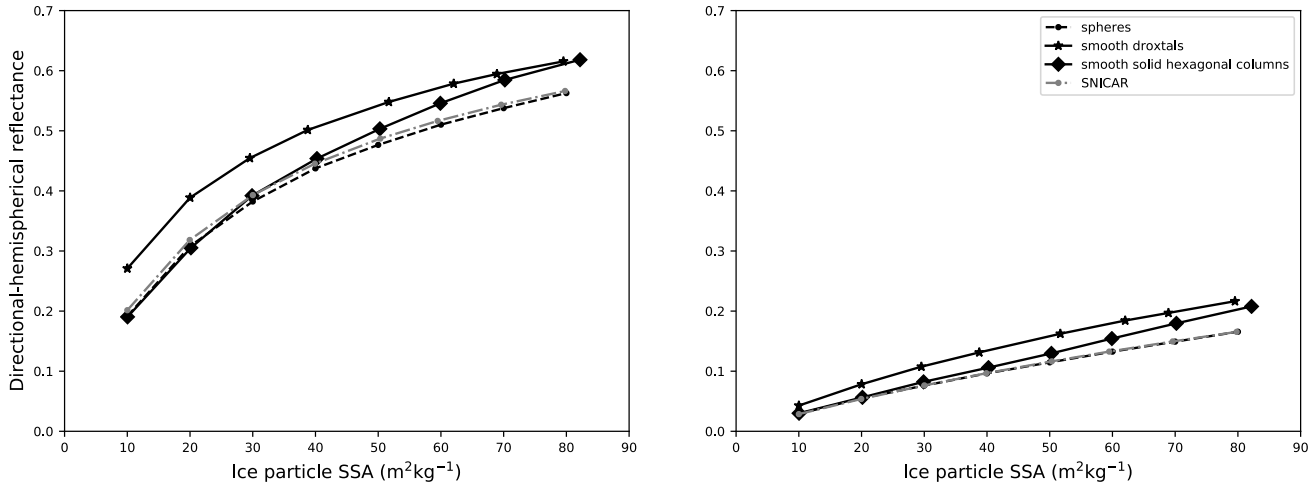

Figure 13. Modeled 1.30 μm nadir (left) and 1.55 μm 15 degree (right) ~~directional-hemispherical~~ directional hemispherical reflectance for various snow SSA. Solid line segments connect albedo calculations from Monte Carlo simulations of light scattering in snow mediums comprised of ~~,~~droxtals (stars) and solid hexagonal columns (diamonds). Circles connected by dashed / dotted line segments connect snow albedo calculations modeled as spherical ice particles; from Monte Carlo modeling (~~light pink~~black) and from the Snow, Ice, and Aerosol Radiation (SNICAR) online model (~~black~~gray).

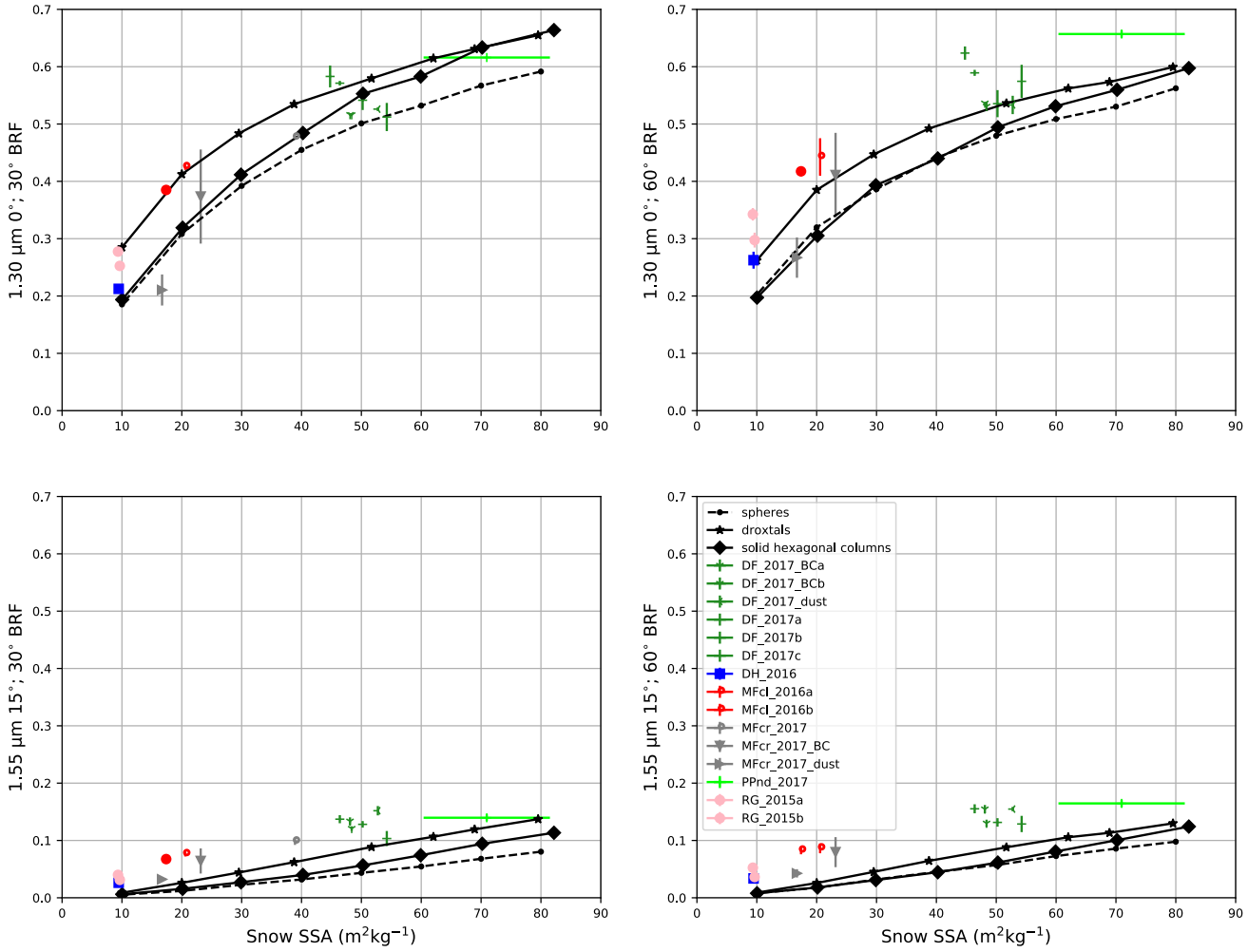

Figure 4. NERD SSA Calibration. All panels contain NERD measured and Monte Carlo modeled (~~connected line segments~~black) ~~modeled~~ BRFs (1.30 µm, top; 1.55 µm, bottom; 30 degrees viewing, left; 60 degrees viewing, right) scattered against snow SSA. NERD BRFs are scattered against X-CT derived snow SSA. Line segments connect Monte Carlo modeled BRFs of snow mediums comprised of spheres (filled circles, dashed lines), droxtals (stars, solid lines), and solid hexagonal columns (diamonds, solid lines). Snow sample key codes, symbols, and colors conform with the physical snow classification standards defined by Fierz et al. (2009) (Table 2). Vertical error bars on NERD BRFs represent standard deviations calculated from multiple azimuthal samples. Horizontal error bars on X-CT derived SSA, where present, represent standard deviations from multiple scans on similar snow samples.

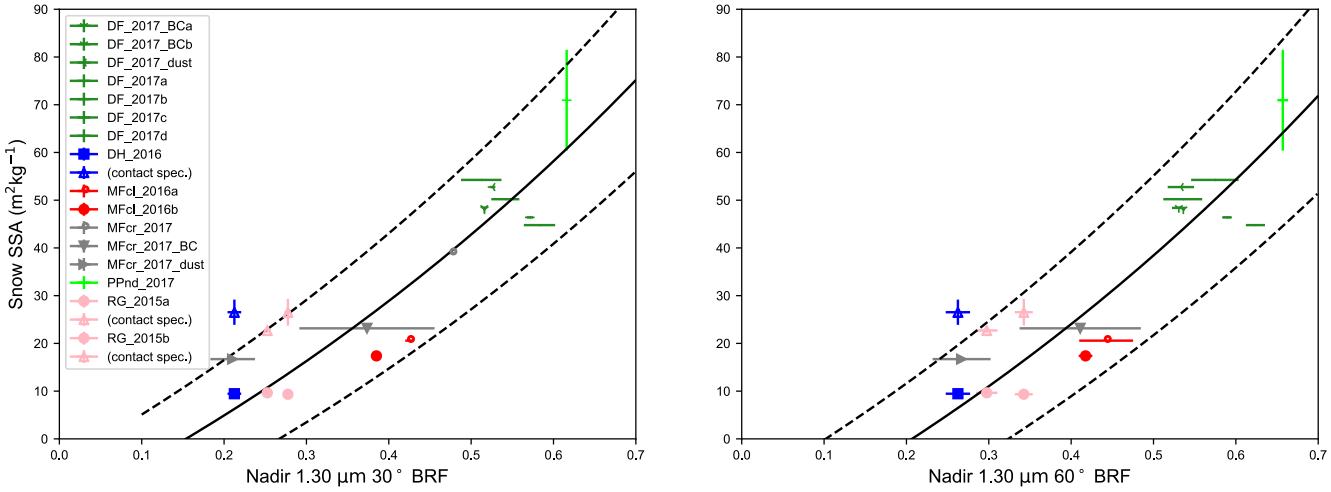

Figure 5. Snow 1.3 µm BRF to SSA exponential regressions. Markers with standard error bars represent SSA, measured with X-CT*, scattered against nadir 1.30 µm 30 (left) and 60 (right) degree BRFs, measured by the NERD. Solid curves represent exponential regression functions and dashed curves represent standard errors of the regressions, such that at 30 degrees viewing, α = 88.7 (+/- 9.50) m^{2}kg^{-1} and β = -103 m^{2}kg^{-1}; and at 60 degrees viewing, α = 91.7 (+/- 10.13) m^{2}kg^{-1} and β = -113 m^{2}kg^{-1}.

*Hollow triangles (blue, depth hoar; pink, rounded grains) represent snow SSA measurements derived from contact spectroscopy.

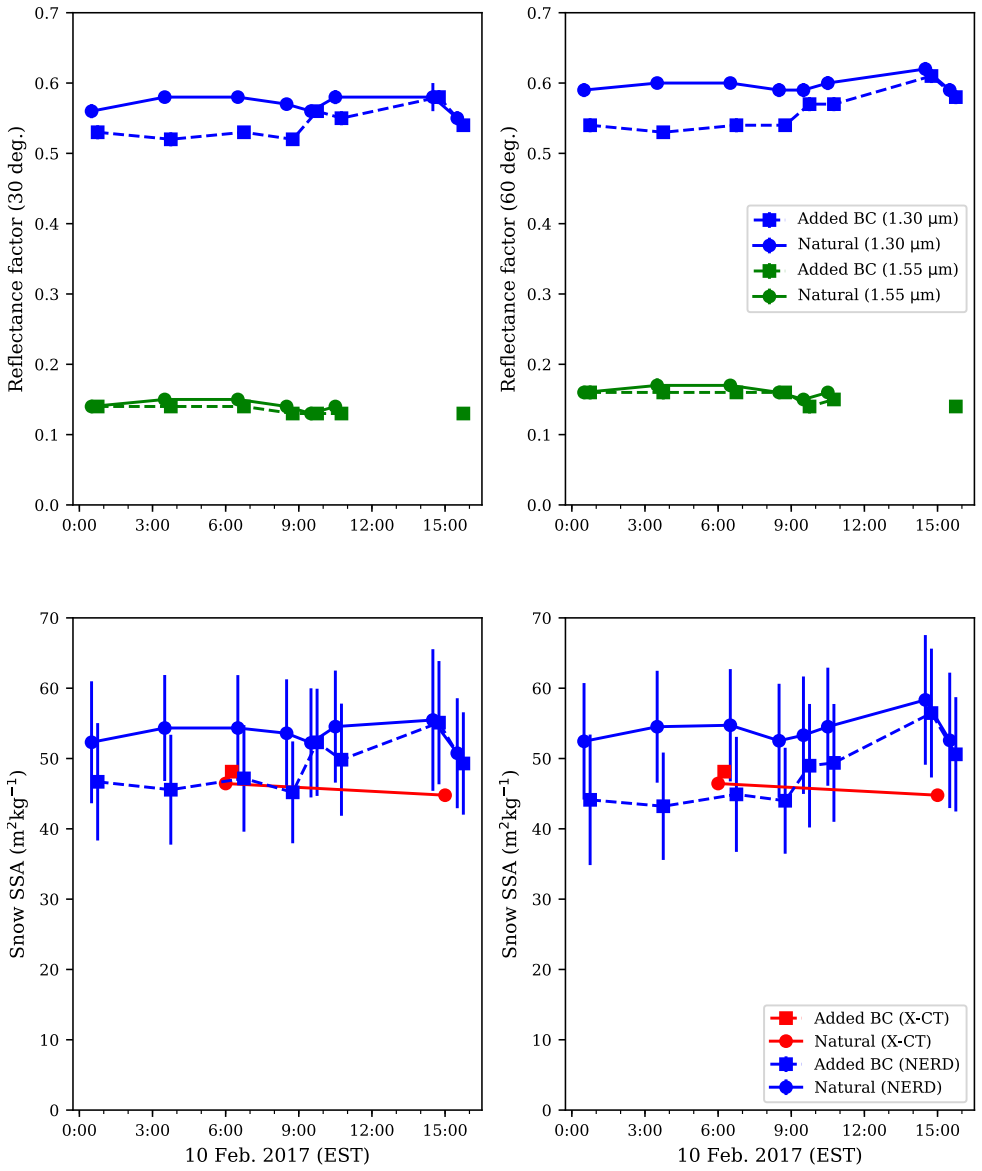

Figure 6. February 10 Control Results (mostly cloudy). All panels contain NERD measurement data collected from ~~12~~00~~:00am~~ 00 through ~~5~~17~~:00pm~~ 00 Eastern Standard Time (EST) on February 10, 2017. Filled circles connected by solid lines represent measurements on natural snow. Filled squares connected by dashed lines represent measurements on snow heavily contaminated by hydrophobic BC. In the top row, blue (green) curves represent 1.30μm (1.55μm) BRFs at 30 degrees viewing – on the left – and 60 degrees viewing – on the right. Error bars represent standard errors calculated from sample averages from as many as eight locations within each square meter plot. In the bottom figure, blue curves represent NERD calibrated SSA from 30, left, and 60, right, degree viewing BRFs. Red curves represent SSA derived from X-CT scans. Error bars represent NERD calibration uncertainty computed from regression analysis (standard errors of the gradients).

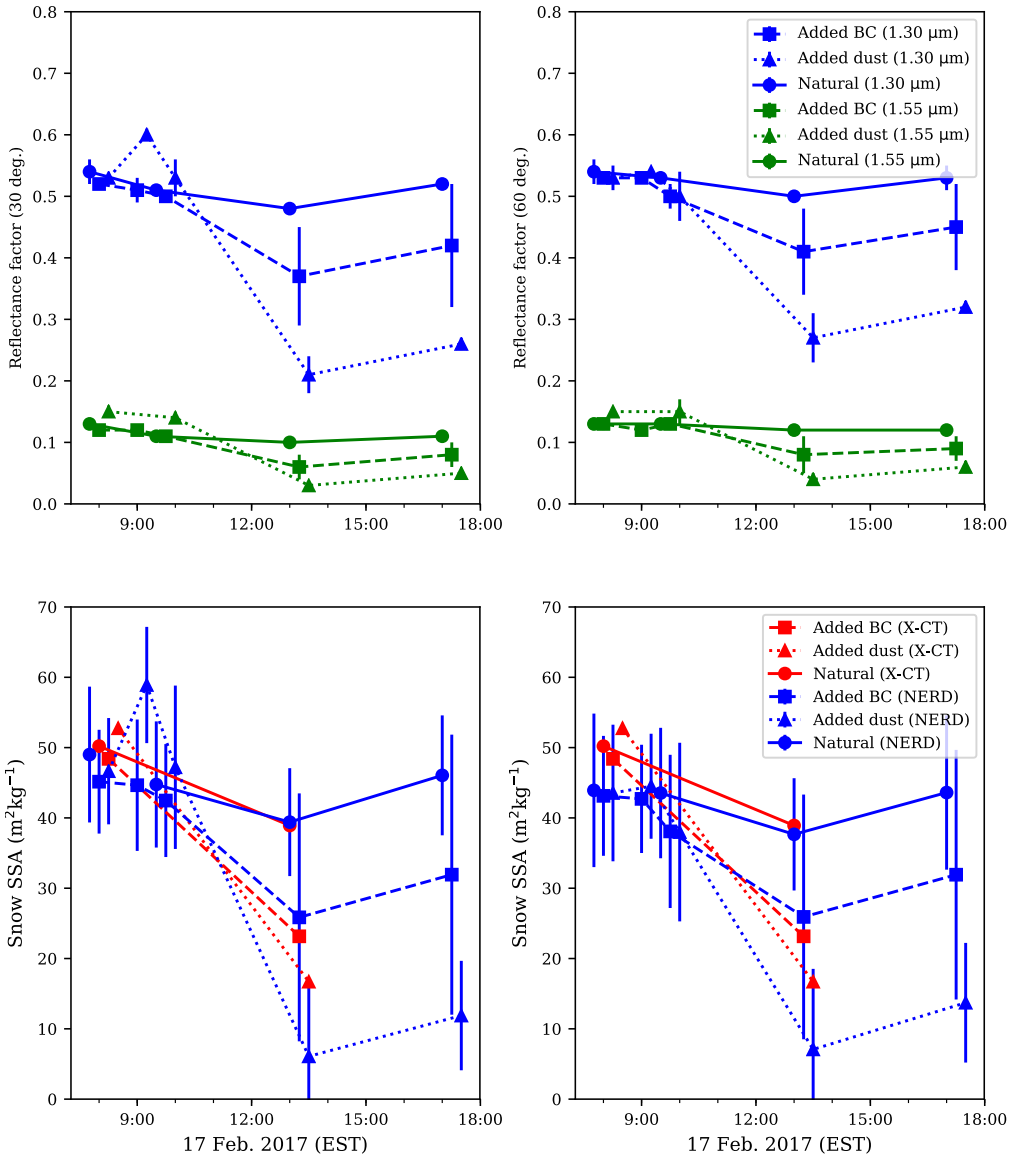

Figure 7. February 17 Experimental Results (clear sky). All panels contain NERD measurement data collected from ~~7~~07~~:00am~~ 00 through 5~~17:00pm~~ 00 EST on February 17, 2017. Filled circles connected by solid lines represent measurements on natural snow. Filled squares connected by dashed lines represent measurements on snow lightly contaminated (< 1 gm^{-1}$^{-2}$) by hydrophobic BC. Triangles connected by dotted lines represent measurements on snow contaminated by ~~sand~~ dust (30 gm^{-1}$^{-2}$). In the top row, blue (green) curves represent 1.30μm (1.55μm) BRFs at 30 degrees viewing – on the left – and 60 degrees viewing – on the right. Error bars represent standard errors calculated from sample averages from as many as eight locations within each square meter plot. In the bottom figure, blue curves represent NERD calibrated SSA from 30, left, and 60, right, degree viewing BRFs. Red curves represent SSA derived from X-CT scans. Error bars represent NERD calibration uncertainty computed from regression analysis (standard errors of the gradients).

Table 1. NERD Lambertian Reflectance Measurements. Tabulated values represent median BRFs ($R(\theta_i;\, \theta_r)$) calculated for n samples of measurements from Lambertian Reflectance targets with nominal reflectances of ρ_L (RMS difference in parenthesis). Linear regressions for each wavelength (λ) are calculated from $n_1 + n_2 = N$ samples.

λ = 1.30 μm					
n	ρ_L	$R(0°; 30°)$	$R(0°; 60°)$	$R(10°; 30°)$	$R(10°; 60°)$
10	0.422	0.399 (0.021)	0.422 (0.016)	0.415 (0.015)	0.434 (0.015)
10	0.951	0.939 (0.013)	0.944 (0.015)	0.958 (0.018)	0.952 (0.010)
N			Linear regression; $\hat{R}(\rho_L) = A\rho_L + B$		
20	$\hat{R} =$	{1.023ρ_L - 0.028,	0.987ρ_L + 0.007,	1.031ρ_L - 0.024,	0.980ρ_L - 0.018}

λ = 1.55 μm					
n	ρ_L	$R(15^\circ_a;30°)$	$R(15^\circ_a;60°)$	$R(15^\circ_b;30°)$	$R(15^\circ_b;60°)$
10	0.413	0.410 (0.009)	0.420 (0.017)	0.411 (0.008)	0.420 (0.021)
6	0.944	0.959 (0.012)	0.963 (0.019)	0.960 (0.013)	0.964 (0.020)
N			Linear regression; $\hat{R}(\rho_L) = A\rho_L + B$		
16	$\hat{R} =$	{1.028ρ_L - 0.016,	1.016ρ_L + 0.003,	1.026ρ_L - 0.014,	1.011ρ_L + 0.009}

Table 2. Snow Sample Physical Classification (Fierz et al., 2009). Snow density, porosity, and specific surface area (SSA) are calculated from X-ray micro-computed tomography.

Grain shape	Density (kg m^{-3})	Porosity (%)	SSA ($m^2 kg^{-1}$)	~~LAI~~ LAPs	Figure key code
Needles	110	88	66	None	PPnd_2017
Decomposing precip. particles	170	82	54	None or w/ dust or BC	DC_2017
Melt-freeze crust	310	66	23	None or w/ dust or BC	MFcr_2017
Clustered rounded grains	350	62	19	None	MFcl_2016
Depth hoar	320	65	9	None	DH_2016
Rounded grains	610	33	9	None	RG_2015